Spherical and cylindrical conductive thermal diodes based on VO2

Suraju Olawale Kasali, Jose Ordonez-Miranda, Karl Joulain

Spherical and cylindrical conductive thermal diodes based on VO_2

Suraju Olawale Kasali,* Jose Ordonez-Miranda, and Karl Joulain
Institut Pprime, CNRS, Université de Poitiers, ISAE-ENSMA, F-86962 Futuroscope Chasseneuil, France
(Dated: October 19, 2018)

We theoretically and comparatively study the performance of spherical and cylindrical conductive thermal diodes operating with a phase-change material, whose thermal conductivity significantly changes in a narrow interval of temperatures. Simple analytical expressions are derived for the temperature profiles, heat fluxes and optimal rectification factors of both diodes. It is shown that the diode geometry has a strong impact on the temperatures and heat fluxes, but not so much on the diode rectification factor. Optimal rectification factors of 20.8% and 20.7% are obtained for the spherical and cylindrical diodes operating with a temperature difference of $376 - 300 = 76$ K and $376.5 - 300 = 76.5$ K between the terminals of VO_2 and a phase invariant material, respectively. These similar rectification factors could be enhanced with a material thermal conductivity exhibiting a faster phase transition and/or higher contrast than that of VO_2. The obtained results can thus be useful to guide the development of phase change materials able to optimize the rectification of conductive thermal diodes with different geometries.

I. INTRODUCTION

Thermal rectification consists in allowing the heat flux between two terminals in a given direction and blocking it in the opposite one, when their temperatures are reversed. This tunning of the heat transport can be achieved through thermal diodes operating with phonons, electrons, and photons. In the last years, an increasing interest has been given to thermal rectification as a result of its potential application in heat control [1]. Recently, theoretical studies of this phenomenon has been carried out based on Phononic [2–7], photon radiation [8–11], electronic [12], and hybrid quantum structures [13]. The effect of this thermal rectification has also been experimentally observed in graphene nanoribbons [14], bulk materials [15], structures of carbon nanotubes [16], oxide materials [17], phase-change materials (PCMs) [18, 19] and quantum dots [20].

Vanadium dioxide (VO_2) has attracted great interest in both theoretical and experimental studies for the past several decades, as result of its hysteretic metal-insulator transition (MIT) [9, 21, 22]. VO_2 undergoes MIT around a critical temperature (~ 340 K) from a low-temperature ($T < 340$ K) semiconducting phase to a high-temperature ($T > 345$ K) metallic one [23, 24]. Interestingly, this MIT is accompanied by drastic changes in its crystal structure from a symmetric monoclinic crystalline to a tetragonal rutile when the temperature is slightly above the critical one [23, 25]. As a result of the transition properties and remarkable change of its lattice structures, VO_2 can be widely used for a variety of applications in electrical and optical devices such as thermal rectifier [26], thermal memory [27], thermal memristor and neuromorphic [28], optical switching [29], hybrid-metamaterial [30], thermal transistor [31] and electrostatic [32].

The concept of thermal rectifier in a plane geometry based on heat conduction of two materials, each of them having a temperature-dependent thermal conductivity was first proposed by Peyrard [33]. However, thermal rectification based on steady-state heat conduction for plane, cylindrical and spherical geometries has been reported by Sadat and Le Dez [34]. On the other hand, a plane geometry conductive thermal diodes based on the thermal hysteresis of PCM and non-PCM has been recently studied by Ordonez-Miranda *et al.* [35]. These two-latter authors derived expressions for heat flux, temperature profiles and rectification factor, however, none of them emphasized on the effect of different geometrical conductive thermal diodes based on VO_2 and non-PCM which are presented in this work.

In this work, we have theoretically demonstrated the effect of spherical and cylindrical conductive thermal diodes based on the thermal rectification of PCM and non-PCM. We have considered two different materials, one driven by temperature-dependent thermal conductivity while the other is constant. Furthermore, we looked at the optimization of the rectification factor of these diodes between the terminals of VO_2 and a phase invariant material. Simple analytical expressions are derived for the temperature profiles, heat fluxes and optimal rectification factor of both diodes supporting steady-state thermal conduction.

*suraju.olawale.kasali@univ-poitiers.fr

II. THEORETICAL MODELING

Let us consider a bilayer spherical thermal shells consisting of the regions (1) and (2) that interchange heat as a result of steady-state thermal conduction between the terminals of VO_2 and non-PCM, respectively. The shells are set such that the temperature T_h in the first region is greater than the temperature T_c of the second one ($T_h > T_c$), as shown in Fig. 1. The forward configuration is the one where the flow of heat flux q_F goes from VO_2 to non-PCM, while in the backward one, the heat flux q_B flows in the reverse direction. The two heat fluxes q_F and q_B are driven by the thermal conductivities $\kappa_1(T)$ in the first region and κ_2 in the second one, as a result, they are expected not to be equal ($q_F \neq q_B$), due to the temperature dependence of $\kappa_1(T)$, for temperatures inside the transition region of the VO_2. For simplicity and clarity sake, we assume that the thermal conductivity κ_2 is independent of temperature in the region (2) for both forward and backward configurations. Hence, it allows optimizing the difference between the two heat fluxes ($q_F - q_B$) as a result of the asymmetry of $\kappa_1(T)$ in the surrounding of its transition temperature T_0 whenever $T_c < T_0 < T_h$.

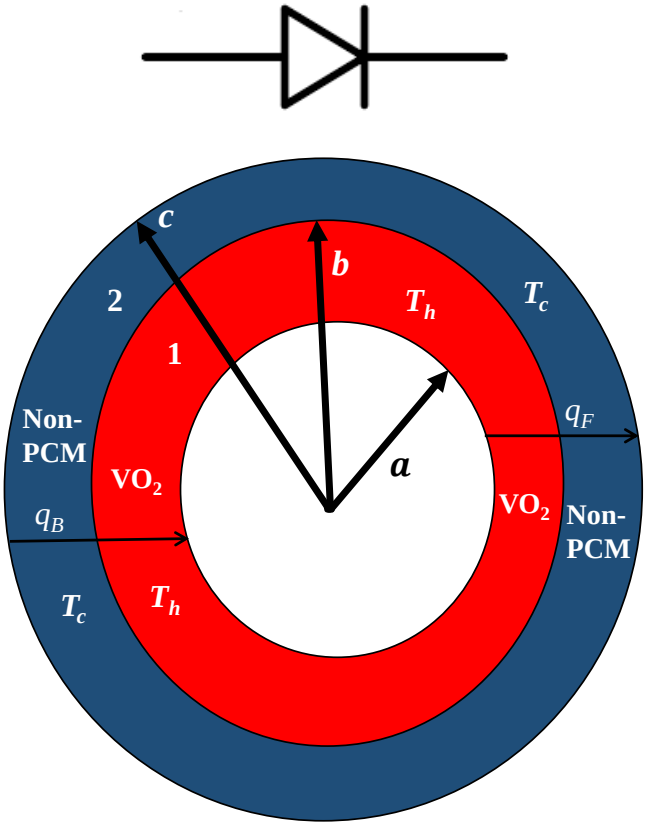

FIG. 1: Schematic diagram of a bilayer conductive thermal diodes consisting of a VO_2 and Non-PCM in the forward and backward configurations, where T_h and T_c are temperatures of hot and cold regions, respectively.

According to [35], the thermal conductivity of VO_2 and non-PCM can be described by

$$\kappa_1(T) = \kappa_d + \frac{\kappa_m - \kappa_d}{1 + e^{-\beta(T-T_0)}}, \tag{1}$$

where $\kappa_m = 6$ $\mathrm{Wm^{-1}K^{-1}}$ and $\kappa_d = 3.6$ $\mathrm{Wm^{-1}K^{-1}}$ are thermal conductivities in their metallic and dielectric states, respectively; $T_0 = 342.5$ K is the transition temperature and $\beta = 1.7$ $\mathrm{K^{-1}}$ is the phase transition slope of $\kappa_1(T)$ when the temperature is equal to the transition one.

A. Spherical diode

1. Forward configuration

According to Fourier's law of thermal conduction, the heat flux q_F in the forward configuration for the spherical diode under steady-state conditions considered in this work is given by

$$q_F = -A(r)\kappa_1(T_1)\frac{dT_1}{dr} = -A(r)\kappa_2\frac{dT_2}{dr}, \tag{2}$$

$$A(r) = 4\pi r^2, \tag{3}$$

where $T_1(r)$ and $T_2(r)$ are the temperatures within the VO_2 and non-PCM regions, respectively.

In order to deduce the parameters as discussed in the previous section, we have considered the following three boundary conditions for forward configuration between the two regions as follows: $T_1(a) = T_h, T_2(c) = T_c$, and $T_1(b) - T_2(b) = R_{12}q_F/4\pi b^2$, with R_{12} being the interface thermal resistance between the VO_2 and non-PCM. In the steady-state regime of heat conduction without losses of generality on the external surface of the junction, the temperature $T_1(r)$ is determined by integrating Eq. (1) with the thermal conductivity in Eq. (3), is given by

$$T_1(r) - T_0 + \frac{1}{\beta\gamma}\ln[1 + \lambda(T_1(r))] = \frac{C}{\kappa_m} + \frac{q_F}{4\pi r\kappa_m}, \tag{4}$$

where $\lambda(T) = \exp[-\beta(T - T_0)]$,$\gamma = \kappa_m/\kappa_m - \kappa_d$ and C is a constant of integration. From Eq. (4), the expressions for the heat flux and temperature profile in the forward configuration are derived by solving for q_F and C using the boundary conditions as stated above, this yields

$$q_F = \frac{1}{\beta\gamma\delta_m}\ln\left[\frac{G(T_h)}{G(T_c + \delta q_F)}\right], \tag{5}$$

$$G(T_1(r)) = [G(T_h)]^{\alpha}[G(T_c + \delta q_F)]^{1-\alpha}, \tag{6}$$

where $\delta_m = \rho/\kappa_m$, $\rho = (b-a)/4\pi ab$, $G(T) = 1+\lambda(T)/[\lambda(T)]^{\gamma}$, and $\alpha = a(b-r)/r(b-a)$. $\delta = [R_{12}+b(c-b)/c\kappa_2]/4\pi b^2$ is the thermal resistance between the non-PCM together with that of the VO_2. It can be seen that the thermal resistance is not the same when compared to the one reported by Ordonez-Miranda *et al.* [35], as $\rho = R_{12} + L_2/\kappa_2$. This results from the difference of the system geometry. Therefore, it is reasonable to say that change of geometry plays a crucial role in the thermal resistance of conductive thermal diodes between the terminals of PCM and invariant one. Furthermore, the temperature profile $T_2(r)$ in the region (2) is derived by integrating the second equality sign of Eq. (1). This yields

$$T_2(r) = T_c + \frac{q_F}{\kappa_2}\sigma(1 - M), \tag{7}$$

where $\sigma = (c - b)/4\pi bc$ and $M = c(r - b)/r(c - b)$.

2. Backward configuration

By following a similar approach as in the forward case, but with a reversed order boundary conditions, that is, to say: $T_1(a) = T_c, T_2(c) = T_h$, and $T_2(b) - T_1(b) = R_{12}q_B/4\pi b^2$. The temperature $T_1(r)$ in the backward configuration is given by

$$T_1(r) - T_0 + \frac{1}{\beta\gamma}\ln[1 + \lambda(T_1(r))] = \frac{D}{\kappa_m} + \frac{q_B}{4\pi r\kappa_m}, \tag{8}$$

where D is a constant of integration. From Eq. (8), by solving for q_B and D using the same procedure as in the forward configuration, the expressions for the heat flux (q_B) and temperature profiles [$T_1(r)$ and $T_2(r)$] are found to be

$$q_B = \frac{1}{\beta\gamma\delta_m}\ln\left[\frac{G(T_h - \delta q_B)}{G(T_c)}\right], \tag{9}$$

$$G(T_1(r)) = [G(T_c)]^{\alpha}[G(T_h - \delta q_B)]^{1-\alpha}. \tag{10}$$

$$T_2(r) = T_h - \frac{q_B}{\kappa_2}\sigma(M-1). \tag{11}$$

B. Cylindrical diode

1. Forward configuration

The heat fluxes and temperature profiles for the forward and backward configurations are derived for the cylindrical diode by using a similar procedure as in the spherical one. In this case, the boundary conditions are slightly different than that of the spherical diode, is given as follows: $T_1(a) = T_h$, $T_2(c) = T_c$, and $T_1(b) - T_2(b) = R_{12}q_F/2\pi bh$. From Fourier's law of thermal conduction, the heat flux (q_F) in the forward configuration is thus given by

$$q_F = -2\pi rh\kappa_1(T_1)\frac{dT_1}{dr} = -2\pi rh\kappa_2\frac{dT_2}{dr}. \tag{12}$$

The integration of Eq. (12) together with Eq. (3) yields the temperature $T_1(r)$, as follow:

$$T_1(r) - T_0 + \frac{1}{\beta\gamma}\ln[1+\lambda(T_1(r))] = \frac{E}{\kappa_m} - \frac{q_F}{2\pi h\kappa_m}\ln r, \tag{13}$$

where E is a constant of integration. The expressions of the heat flux (q_F) and temperature profile $T_1(r)$ are determined by solving Eq. (13) for both q_F and E at the temperature conditions as state above, which results to

$$q_F = \frac{1}{\beta\gamma\mu_m}\ln\left[\frac{G(T_h)}{G(T_c+\mu q_F)}\right], \tag{14}$$

$$G(T_1(r)) = [G(T_h)]^J[G(T_c+\mu q_F)]^{1-J}, \tag{15}$$

where $\mu_m = Z/\kappa_m$, $Z = \ln(b-a)/2\pi h$, and $J = \ln(b-r)/\ln(b-a)$. $\mu = [R_{12} + b\ln(c-b)/\kappa_2]/2\pi bh$ is the thermal resistance of the non-PCM combined with that of VO_2. It can also be seen that the thermal resistance of the cylindrical diode is not the same when compared to that of the spherical one, as well as that of the plane one reported by Ordonez-Miranda *et al.* [35]. As a result, one can say that the change of geometry has a significant impact on the measure of resistance to thermal flow between the terminals of VO_2 and non-PCM. On the other hand, the temperature profile $T_2(r)$ in the second region is determined by integrating the equality sign of the second part of Eq. (12), which gives

$$T_2(r) = T_c + \frac{q_F}{\kappa_2}Q(1-V), \tag{16}$$

where $Q = \ln(c-b)/2\pi h$ and $V = \ln(r-b)/\ln(c-b)$.

2. Backward configuration

The temperature $T_1(r)$ in the backward configuration of the cylindrical diode is determined by following similar process as in the forward case, but with the boundary conditions in a reversed order as follows: $T_1(a) = T_c, T_2(a) = T_h$, and $T_2(b) - T_1(b) = R_{12}q_B/2\pi bh$. The expression is found to be

$$T_1(r) - T_0 + \frac{1}{\beta\gamma}\ln[1+\lambda(T_1(r))] = \frac{F}{\kappa_m} - \frac{q_B}{2\pi h\kappa_m}\ln r, \tag{17}$$

where F is an integration constant. The expressions for the heat flux (q_B) and the temperature profiles [$T_1(r)$ and $T_2(r)$] can be determined by following a similar procedure as in the forward case. The final results are

$$q_B = \frac{1}{\beta\gamma\mu_m}\ln\left[\frac{G(T_h-\mu q_B)}{G(T_c)}\right], \tag{18}$$

$$G(T_1(r)) = [G(T_c)]^J[G(T_h-\mu q_B)]^{1-J}, \tag{19}$$

$$T_2(r) = T_h - \frac{q_B}{\kappa_2}Q(V-1). \tag{20}$$

C. Rectification factor

Following previous research [36], the rectification factor τ can be defined as the ratio of the difference between the forward and backward heat fluxes to the maximum of the heat fluxes, which is given by

$$\tau = \frac{|q_F - q_B|}{\max(q_F, q_B)} = 1 - \frac{q_{B,\min}}{q_{F,\max}}. \tag{21}$$

The important step in the evaluation of Eq. (21) is to determine the expressions for the maximum value of q_F and minimum of q_B for both diodes. This fact can be easily analyzed by rewriting Eqs. (5) and (9), as follows:

$$q_F = \frac{T_h - T_c}{\delta + \delta_m} + (\beta\gamma(\delta + \delta_m))^{-1} \ln\left[\frac{1 + \lambda(T_h)}{1 + \lambda(T_c)e^{-\beta\delta q_F}}\right], \tag{22}$$

$$q_B = \frac{T_h - T_c}{\delta + \delta_m} - (\beta\gamma(\delta + \delta_m))^{-1} \ln\left[\frac{1 + \lambda(T_c)}{1 + \lambda(T_h)e^{\beta\delta q_B}}\right]. \tag{23}$$

Given that in Eqs. (22) and (23) the fraction quantities inside the natural logarithm are greater than or equal to 1, this show that q_F is less than or equal to $(T_h - T_c)/(\delta + \delta_m)$. However, further simplification of the term $q_B(\beta\gamma(\delta+\delta_m))^{-1}$ in Eq. (23) show that the backward heat flux q_B is greater than or equal to $(T_h - T_c)/(\delta + \delta_d)$. This is similar to what was proposed by Ordonez-Miranda *et al.* [35], but with different thermal resistances ($\delta_m = \rho/\kappa_m$ and $\delta_d = \rho/\kappa_d$), because of difference of the system geometry. One should note that here a similar result is expected, since the same model for thermal conductivity of VO_2 and non-PCM is employed. Furthermore, if we consider the fact that $T_c < T_0 < T_h$ and $\beta = 1.7$ K^{-1} as mentioned in the previous section, this implies that the maximum of q_F in Eq. (22) is obtained whenever $T_h - T_c \gg \beta^{-1}$ and $T_c - T_0 + \delta q_F \gg \beta^{-1}$, so, therefore, Eq. (22) becomes

$$q_{F,\max} = \frac{T_h - T_c}{\delta + \delta_m}. \tag{24}$$

Further simplification of the terms $T_h - T_c \gg \beta^{-1}$ and $T_c - T_0 + \delta q_F \gg \beta^{-1}$, yields, $T_h - T_0 \gg (T_0 - T_c)\delta_m/\delta + (1 + \delta_m/\delta)\beta^{-1}$, which is valid for all $T_0 > T_c$. On the contrary, the minimum expression for the q_B in Eq. (23) is obtained whenever $T_0 - T_c \gg \beta^{-1}$ and $T_h - T_0 - \delta q_B \gg \beta^{-1}$, the result is given by

$$q_{B,\min} = \frac{T_h - T_c - \varphi}{\delta + \delta_m}, \tag{25}$$

where $\varphi = (T_0 - T_c)/\gamma$. The result of the optimal rectification factor τ_{opt} can be found by substituting Eqs. (24) and (25) into Eq. (21). This yields

$$\tau_{opt} = \left(\frac{T_0 - T_c}{T_h - T_c}\right)\gamma^{-1}. \tag{26}$$

Equation (26) satisfies the condition for temperature $T_c < T_0 < T_h$ and for different values of the thermal resistances δ, δ_m, and δ_d of the spherical diode. Since T_0 is constant, τ_{opt} can be estimated for VO_2 and non-PCM by varying T_c and T_h, respectively. The optimal rectification factor for the cylindrical diode can be found by following a similar procedure as in the latter case. This is done by rewriting Eqs. (14) and (18), as follows:

$$q_F = \frac{T_h - T_c}{\mu + \mu_m} + (\beta\gamma(\mu + \mu_m))^{-1} \ln\left[\frac{1 + \lambda(T_h)}{1 + \lambda(T_c)e^{-\beta\mu q_F}}\right], \tag{27}$$

$$q_B = \frac{T_h - T_c}{\mu + \mu_m} - (\beta\gamma(\mu + \mu_m))^{-1} \ln\left[\frac{1 + \lambda(T_c)}{1 + \lambda(T_h)e^{\beta\mu q_B}}\right]. \tag{28}$$

It can be seen easily that Eqs. (22) and (23) of the spherical diode is different from Eqs. (27) and (28) of the cylindrical one by the following thermal resistances δ, δ_m, μ, and μ_m, respectively. Therefore, it follows that the optimal rectification factor τ_{opt} given by Eq. (26) is the same for both diodes and as well satisfies the same condition for temperature $T_c < T_0 < T_h$ and for different values of the thermal resistances μ, μ_m, and μ_d of the cylindrical diode. This fact is in good agreement with the optimal rectification factor in a plane diode reported by Ordonez-Miranda *et al.* [35], but with different thermal resistance as compared to what is proposed in this work. These results fairly agree with the fact proposed by Ordonez-Miranda *et al.* [35], that the increase or decrease in thermal resistance has an insignificant impact on the enhancement of τ. However, because of the difference in the respective thermal resistances, the conditions that must be satisfied for $q_{F,\max}$ and $q_{B,\min}$ in the cylindrical diode differ, and are given as follows: $T_0 - T_c \gg \beta^{-1}$ and $T_h - T_0 - \mu q_B \gg \beta^{-1}$ for $q_{B,\min}$, $T_h - T_c \gg \beta^{-1}$ and $T_c - T_0 + \mu q_F \gg \beta^{-1}$ for $q_{F,\max}$.

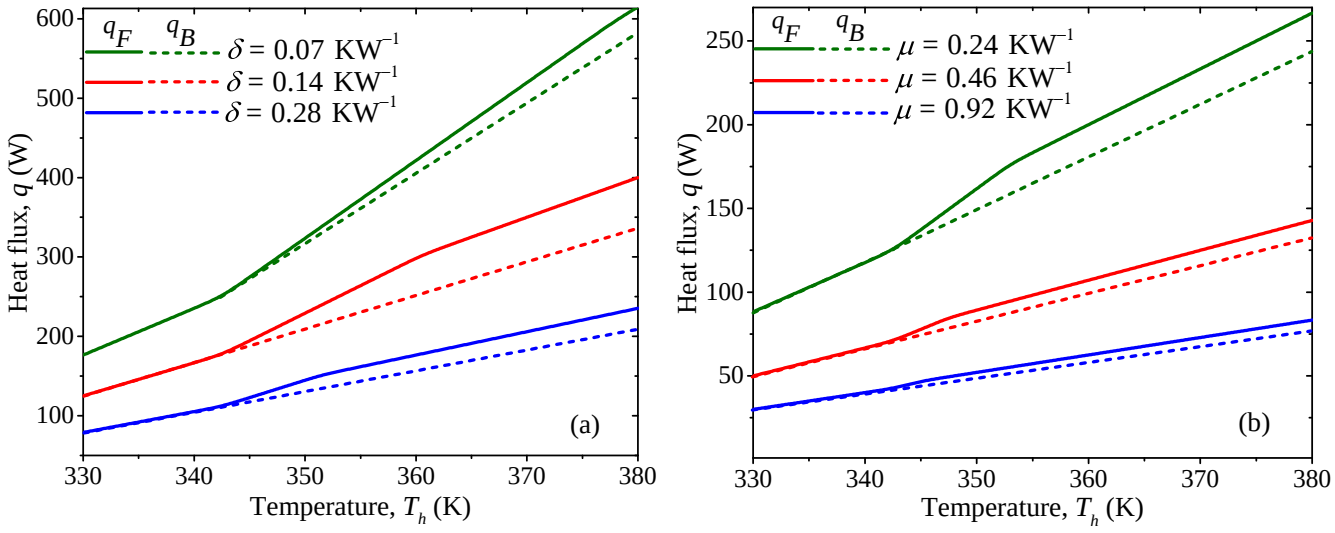

FIG. 2: Heat fluxes in the conductive thermal diode of VO_2 and non-PCM for (a) spherical and (b) cylindrical diodes in the forward and backward configurations. Calculations have been done for three representative interface thermal resistances.

III. RESULTS AND DISCUSSION

The heat fluxes q_F and q_B for the forward and backward configurations within a conductive thermal diode operating between the terminals of PCM and an invariant one are depicted in Figs 2(a) and 2(b), respectively. It can be seen that the values of the three respective thermal resistances in both diodes result in such that the heat flux in the forward configuration is higher than the one of the backward ($q_F > q_B$) such that their difference lean towards a constant value for the temperature of the hotter regime T_h much higher than the transition one, where VO_2 exhibits its tetragonal rutile phase. This is expected following the behavior of the thermal diode, which minimized the heat flux in the reversed direction, and as well as with the prediction of Eqs. (24) and (25). It can also be seen that the lowest thermal resistances in both diodes generate the highest heat fluxes. This is consistent with the fact that Eqs. (5), (9), (14) and (18) has a very strong non-linear dependence of T_h and T_c with the thermal resistance as a coefficient of the heat flux, this can be seen in the denominator of expressions inside the logarithm function. It is expected following the relationship between thermal resistance and heat conductance proposed by Marin [37], as $R_{cond.} = 1/h_{cond.}$. Our results agree well with literature hysteresis [9, 22], that VO_2 exhibits a dielectric-to-metal transition at a critical temperature (~ 340 K). Our results also agree with what was proposed by [38–40] that thermal resistance influences the heat transfer mechanism. It can also be seen that in the spherical diode, the values of heat flux generated are higher than that of the cylindrical one. This is expected following that the thermal resistance δ in the spherical diode is less than μ in the cylindrical one. Therefore, it is reasonable to conclude that difference of the system geometry which leads to an influence of the thermal resistances has a significant impact on the heat fluxes and temperature profiles of a conductive thermal diode in the steady-state regime of heat conduction.

It is worth pointing out the impact of these geometrical diodes on the rectification factor. As a result, we have shown in Figs. 3(a) and 3(b) the plots of conductive thermal diodes operating within the shell of VO_2 and non-PCM over sapphire for both diodes with respect to temperature T_h of the hotter region, respectively. It can be seen that for all thermal resistance values in both cases, the rectification factor vanishes at the temperatures where the forward and backward heat fluxes are equal ($q_F = q_B$), this is similar to what is shown in Figs. 2(a) and 2(b). Nevertheless, the spherical and cylindrical diodes of thermal resistance $\delta = 0.28$ KW^{-1} and $\mu = 0.24$ KW^{-1} generate the highest optimal rectification factor of $\tau_{opt} = 20.8\%$ and $\tau_{opt} = 20.7\%$ with temperature $T_h = 376$ K and $T_h = 376.5$ K, respectively. This is also consistent with the variation in the size of the materials a, b and c in both cases. The highest value of the size of these materials generates maximum optimal rectification factor, this fairly agrees with the result in the spherical diode. However, the lowest value generates the uppermost rectification factor, which corresponds to the result in the cylindrical one. Furthermore, the density plot in Figs. 4(a) and 4(b) show the actualization of these optimal thermal resistances ($\delta = [R_{12} + b(c-b)/c\kappa_2]/4\pi b^2$, and $\mu = [R_{12} + b\ln(c-b)/\kappa_2]/2\pi bh$) and the temperatures of the hotter shell (T_h), this indicates that the increase or decrease in δ and μ does not necessarily denote the enhancement of rectification factor τ. Following the predictions of Eq. (26) these results show that between the terminals of

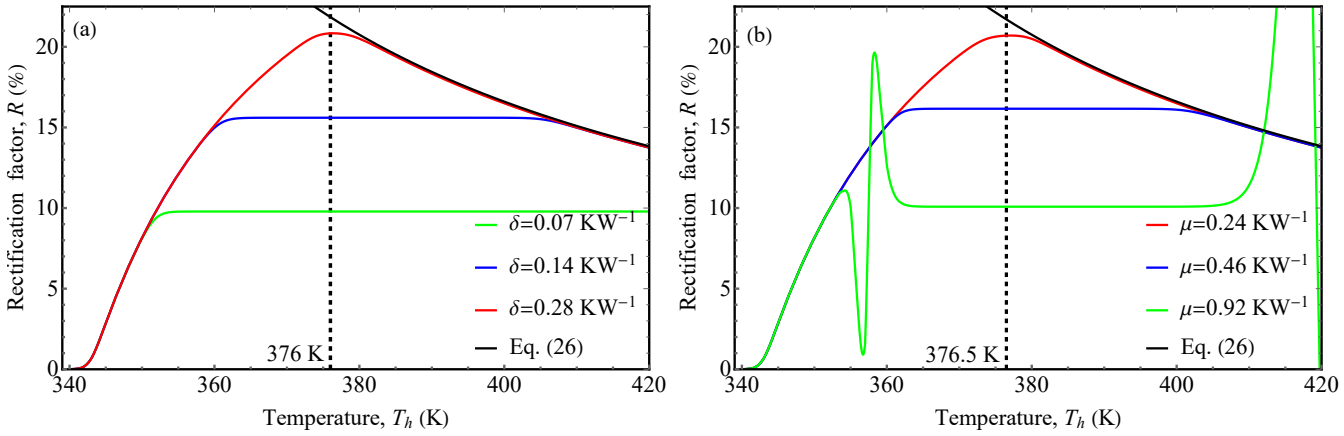

FIG. 3: Rectification factor of the conductive thermal diode for (a) spherical and (b) cylindrical diodes. Calculations are done for different values of the three interface thermal resistances.

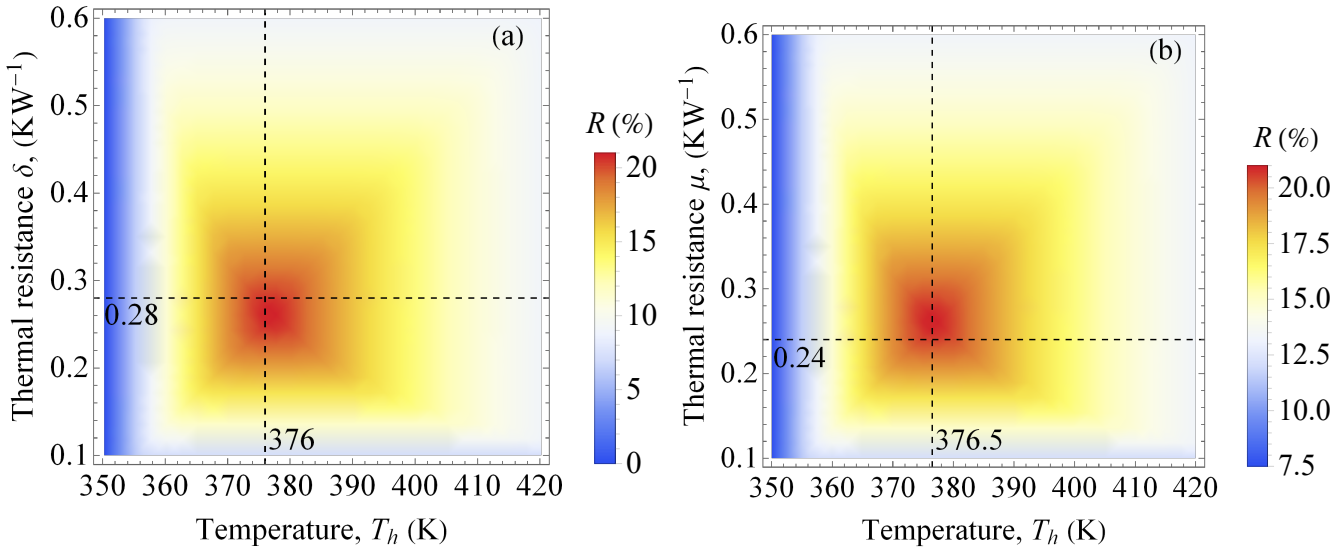

FIG. 4: Rectification factor for the (a) spherical and (b) cylindrical diodes, as functions of the temperature T_h.

PCM and a phase invariant one, the spherical and cylindrical diodes generate the same τ_{opt}. These results agree well with what was reported by Ordonez-Miranda *et al.* [35]. On the contrary, the temperature ranges ($376 - 300 = 76$ K) and ($376.5 - 300 = 76.5$ K) of both diodes presented in this work are higher than the value ($369.5 - 300 = 69.5$ K) for VO_2 and less than ($388.2 - 273 = 115.2$ K) for nitinol as proposed by Ordonez-Miranda *et al.* [35]. Our results as well agree with the fact that the temperature required by VO_2 to reach the maximum rectification factor is less than that of nitinol, which is due to the fact that VO_2 has a rapid phase transition when compared to nitinol.

IV. CONCLUSIONS

We have theoretically investigated and optimized the rectification factor of a spherical and cylindrical conductive thermal diodes between the terminals of phase-change material and a phase invariant one. This is done by deriving simple analytical expressions for the temperature profiles, heat fluxes and optimal rectification factor of both diodes. It has been shown that the diode geometry has a significant impact on the temperatures and heat fluxes, but not so much on the diode rectification factor. Optimal rectification factors of up to 20.8% and 20.7% have been determined for the spherical and cylindrical diodes operating with a temperature lengths of 76 K and 76.5 K, respectively. The obtained results will serve as a useful guide for the enhancement of phase-change materials able to optimize the

rectification of conductive thermal diodes with different geometries.

[1] N. A. Roberts and D. Walker, Int. J. Therm. Sci. **50**, 648 (2011).
[2] B. Li, L. Wang, and G. Casati, Phys. Rev. Lett. **93**, 184301 (2004).
[3] B. Hu, D. He, L. Yang, and Y. Zhang, Phys. Rev. E **74**, 060101 (2006).
[4] E. Pereira, Phys. Rev. E **83**, 031106 (2011).
[5] G. Zhang and Y.-W. Zhang, Chin. Phys. B **26**, 034401 (2017).
[6] K. Garcia-Garcia and J. Alvarez-Quintana, Int. J. Therm. Sci. **81**, 76 (2014).
[7] G. Zhang and H. Zhang, Nanoscale **3**, 4604 (2011).
[8] K. Joulain, Y. Ezzahri, J. Drevillon, B. Rousseau, and D. D. S. Meneses, Opt. Express **23**, A1388 (2015).
[9] J. Ordonez-Miranda, Y. Ezzahri, J. Drevillon, and K. Joulain, Phys. Rev. Appl. **6**, 054003 (2016).
[10] P. Ben-Abdallah and S.-A. Biehs, Appl. Phys. Lett. **103**, 191907 (2013).
[11] E. Nefzaoui, J. Drevillon, Y. Ezzahri, and K. Joulain, Appl. Opt. **53**, 3479 (2014).
[12] D. Segal, Phys. Rev. Lett. **100**, 105901 (2008).
[13] L.-A. Wu and D. Segal, Phys. Rev. Lett. **102**, 095503 (2009).
[14] J. Hu, X. Ruan, and Y. P. Chen, Nano lett. **9**, 2730 (2009).
[15] D. Sawaki, W. Kobayashi, Y. Moritomo, and I. Terasaki, Appl. phys. lett. **98**, 081915 (2011).
[16] C. Chang, D. Okawa, A. Majumdar, and A. Zettl, Science **314**, 1121 (2006).
[17] W. Kobayashi, Y. Teraoka, and I. Terasaki, Appl. Phys. Lett. **95**, 171905 (2009).
[18] P. Van Zwol, L. Ranno, and J. Chevrier, Phys. Rev. Lett. **108**, 234301 (2012).
[19] Y. Yang, S. Basu, and L. Wang, Appl. Phys. Lett. **103**, 163101 (2013).
[20] R. Scheibner, M. König, D. Reuter, A. Wieck, C. Gould, H. Buhmann, and L. Molenkamp, New J. Phys. **10**, 083016 (2008).
[21] K. Joulain, Y. Ezzahri, J. Drevillon, and P. Ben-Abdallah, Appl. Phys. Lett. **106**, 133505 (2015).
[22] S. Lee, K. Hippalgaonkar, F. Yang, J. Hong, C. Ko, J. Suh, K. Liu, K. Wang, J. J. Urban, X. Zhang, et al., Science **355**, 371 (2017).
[23] M. M. Qazilbash, A. Schafgans, K. Burch, S. Yun, B. Chae, B. Kim, H.-T. Kim, and D. Basov, Phys. Rev. B **77**, 115121 (2008).
[24] J. Ordonez-Miranda, Y. Ezzahri, K. Joulain, J. Drevillon, and J. Alvarado-Gil, Phys. Rev. B **98**, 075144 (2018).
[25] H. Wang, X. Yi, S. Chen, and X. Fu, Sens. Actuator A-Phys. **122**, 108 (2005).
[26] K. Ito, K. Nishikawa, H. Iizuka, and H. Toshiyoshi, Appl. Phys. Lett. **105**, 253503 (2014).
[27] K. Ito, K. Nishikawa, and H. Iizuka, Appl. Phys. Lett. **108**, 053507 (2016).
[28] P. Ben-Abdallah, AIP Adv. **7**, 065002 (2017).
[29] M. Rini, Z. Hao, R. Schoenlein, C. Giannetti, F. Parmigiani, S. Fourmaux, J. Kieffer, A. Fujimori, M. Onoda, and S. Wall, Appl. Phys. Lett. **92**, 181904 (2008).
[30] T. Driscoll, S. Palit, M. M. Qazilbash, M. Brehm, F. Keilmann, B.-G. Chae, S.-J. Yun, H.-T. Kim, S. Cho, N. M. Jokerst, et al., Appl. Phys. Lett. **93**, 024101 (2008).
[31] J. Ordonez-Miranda, Y. Ezzahri, J. Drevillon, and K. Joulain, J. Appl. Phys. **119**, 203105 (2016).
[32] M. M. Qazilbash, Z. Li, V. Podzorov, M. Brehm, F. Keilmann, B. Chae, H.-T. Kim, and D. Basov, Appl. Phys. Lett. **92**, 241906 (2008).
[33] M. Peyrard, Europhys. Lett. **76**, 49 (2006).
[34] H. Sadat and V. Le Dez, Mech. Res. Commun. **76**, 48 (2016).
[35] J. Ordonez-Miranda, J. M. Hill, K. Joulain, Y. Ezzahri, and J. Drevillon, J. Appl. Phys. **123**, 085102 (2018).
[36] J. Ordonez-Miranda, K. Joulain, D. De Sousa Meneses, Y. Ezzahri, and J. Drevillon, J. Appl. Phys. **122**, 093105 (2017).
[37] E. Marin, *Time Varying Heat Conduction in Solids* (InTech, 2013).
[38] R.-C. Chen, J.-P. Wu, and H.-S. Chu, J. Heat Transfer **117**, 366 (1995).
[39] M. Flik, P. Phelan, and C. Tien, Cryogenics **30**, 1118 (1990).
[40] P. E. Phelan, J. Heat Transfer **120**, 37 (1998).